

RESEARCH ARTICLE

Kinesin-1 sorting in axons controls the differential retraction of arbor terminals

Takeshi Seno¹, Tatsuki Ikeno¹, Kousuke Mennya¹, Masayuki Kurishita¹, Narumi Sakae¹, Makoto Sato^{2,3,4,5}, Hiroki Takada¹ and Yoshiyuki Konishi^{1,2,6,*}

ABSTRACT

The ability of neurons to generate multiple arbor terminals from a single axon is crucial for establishing proper neuronal wiring. Although growth and retraction of arbor terminals are differentially regulated within the axon, the mechanisms by which neurons locally control their structure remain largely unknown. In the present study, we found that the kinesin-1 (Kif5 proteins) head domain (K5H) preferentially marks a subset of arbor terminals. Time-lapse imaging clarified that these arbor terminals were more stable than others, because of a low retraction rate. Local inhibition of kinesin-1 in the arbor terminal by chromophore-assisted light inactivation (CALI) enhanced the retraction rate. The microtubule turnover was locally regulated depending on the length from the branching point to the terminal end, but did not directly correlate with the presence of K5H. By contrast, F-actin signal values in arbor terminals correlated spatiotemporally with K5H, and inhibition of actin turnover prevented retraction. Results from the present study reveal a new system mediated by kinesin-1 sorting in axons that differentially controls stability of arbor terminals.

KEY WORDS: Axon, Retraction, Transport, Kinesin, Microtubule, F-actin

INTRODUCTION

To connect with multiple target cells, neurons elaborate the axonal arbor by controlling growth and retraction during development (Gibson and Ma, 2011; Kalil and Dent, 2014). Previous *in vivo* (Portera-Cailliau et al., 2005; Hua et al., 2005; Meyer and Smith, 2006; Stettler et al., 2006; Nishiyama et al., 2007) and *in vitro* (Bastmeyer and O'Leary, 1996; Ruthel and Hollenbeck, 2000) studies have revealed the diverse plasticity of arbor terminals in a single axon. The competition between different terminals of a single axon in cultured neurons (Hutchins and Kalil, 2008) suggests that neurons possess an intracellular system that coordinates the branched axonal shape by regulating growth and retraction of arbor terminals in a region-specific manner. Despite intensive

studies on the axonal arborization, little is known about the intracellular mechanisms mediating terminal-dependent control of growth and retraction in the axonal arbor.

In collateral branch formation, filopodial and lamellipodial protrusions, which contain F-actin bundles, emerge from actin patches found along the axon shaft. Newly formed branches are then invaded by microtubules to become mature axonal branches (Gallo and Letourneau, 1999; Gallo, 2011; Lewis et al., 2013). It is thought that the balance between stabilization and destabilization of F-actin and microtubules determines the formation and growth of axonal branches. For example, activation of the actin nucleation factors, Arp2/3 and Cordon-bleu (Cobl) is required for filopodia formation from the actin patch, and inhibition of this pathway results in decreased branch number (Strasser et al., 2004; Ahuja et al., 2007; Spillane et al., 2011, 2012). The microtubule-severing enzymes, spastin and katanin, which provide a branching point at the axonal shaft, also control the number of axonal branches (Yu et al., 2008). In contrast, neurons that lack Kif2a, a kinesin family molecule that depolymerizes microtubules, exhibit increased axonal branch length (Homma et al., 2003). Thus, local control of F-actin and microtubule dynamics is crucial for shaping the axonal arbor. Nevertheless, intracellular systems that regulate individual arbor terminals in the axon have not been fully demonstrated.

Ca²⁺ is a major intracellular signaling molecule that regulates axonal growth (Kater and Mills, 1991; Gomez and Spitzer, 1999; Tang and Kalil, 2005; Ageta-Ishihara et al., 2009). Previous studies have suggested that localized Ca²⁺ transients in restricted areas in the arbor enhance axonal growth, accompanied by retraction of other terminals (Hutchins and Kalil, 2008). Cyclic nucleotides are thought to be candidates that send long-range signals mediating the competition (Hutchins, 2010), given that in axonal specification, the activation of cAMP in a single neurite mutually inhibits cAMP in other neurites to form a single axon (Shelly et al., 2010). The molecular mechanisms whereby these signals coordinately regulate extension or retraction of different arbor terminals have not been elucidated.

Kinesin-driven anterograde transport along microtubules has been shown to play crucial roles in maintaining axonal morphology and function (Goldstein, 2001; Hirokawa and Takemura, 2005; Salinas et al., 2008; Maday et al., 2014). Conventional kinesin (kinesin-1) consists of heavy chain (Kif5a, Kif5b or Kif5c) dimer and light chains. Kif5 proteins contains a motor domain (also called the head domain) that hydrolyzes ATP and moves along microtubules, whereas the C-terminal tail domain is required for cargo interactions. Because the tail domain inhibits motor function when not bound to cargos, deleting the tail domain results in constitutive activation of Kif5 (Coy et al., 1999). Intriguingly, the cleaved motor (head) domain of Kif5 (K5H) is selectively delivered to axons, but not dendrites (Nakata and Hirokawa, 2003; Jacobson et al., 2006), indicating that K5H has the ability to discriminate

¹Department of Human and Artificial Intelligence Systems, University of Fukui, Fukui 910-8507, Japan. ²Life Science Innovation Center, University of Fukui, Fukui 910-8507, Japan. ³Research Center for Child Mental Development, University of Fukui, Fukui 910-1193, Japan. ⁴Department of Anatomy and Neuroscience, Graduate School of Medicine, Osaka University, Osaka 565-0871, Japan. ⁵United Graduate School of Child Development, Osaka University, Kanazawa University-Hamamatsu University School of Medicine, Chiba University and University of Fukui, Osaka University, Osaka 565-0871, Japan. ⁶Department of Materials Science and Biotechnology, Faculty of Engineering, University of Fukui, Fukui 910-8507, Japan.

*Author for correspondence (ykonishi@u-fukui.ac.jp)

© T.S., 0000-0001-8072-1796; T.I., 0000-0002-3469-4763; M.K., 0000-0003-0775-5433; N.S., 0000-0002-7960-9227; Y.K., 0000-0001-7594-9921

between axons and dendrites. The control of microtubule dynamics has been shown to depend on the region within the single cell (Witte et al., 2008), and microtubule dynamics affect tubulin states, such as GDP or GTP binding, acetylation and tyrosination or dephosphorylation, and decoration by microtubule-associated proteins (MAPs). Recent results from several reports, including from our group, have suggested that K5H recognizes differences between microtubules on axon and dendrites (Reed et al., 2006; Konishi and Setou, 2009; Hammond et al., 2010; Nakata et al., 2011). Nevertheless, very little is known about the regulation of axonal transport within the arbor. Therefore, in the current study, we asked whether there is any difference in efficiency of kinesin-1-dependent axonal transport between terminals of a single axonal arbor. Results showed a selective K5H accumulation in a subset of axonal

terminals, which contributed to the shape of the axonal arbor by differentially regulating retraction.

RESULTS

Kinesin-1 preferentially accumulates in a subset of axonal terminals

To study terminal dependency of kinesin-1-mediated axonal transport, we utilized cerebellar granule neurons (CGNs) that possess relatively simple axonal arbors (Bilimoria et al., 2010; Ito-Ishida et al., 2012). In culture, CGNs extend one or two axons that possess several arbor terminals (Bilimoria et al., 2010; Kubota et al., 2013) (Fig. 1A), thus are thought to be suitable for studying the diversity of arbor terminals. During the axonal arborization of CGNs *in vitro*, elimination of main axon terminal as well as massive

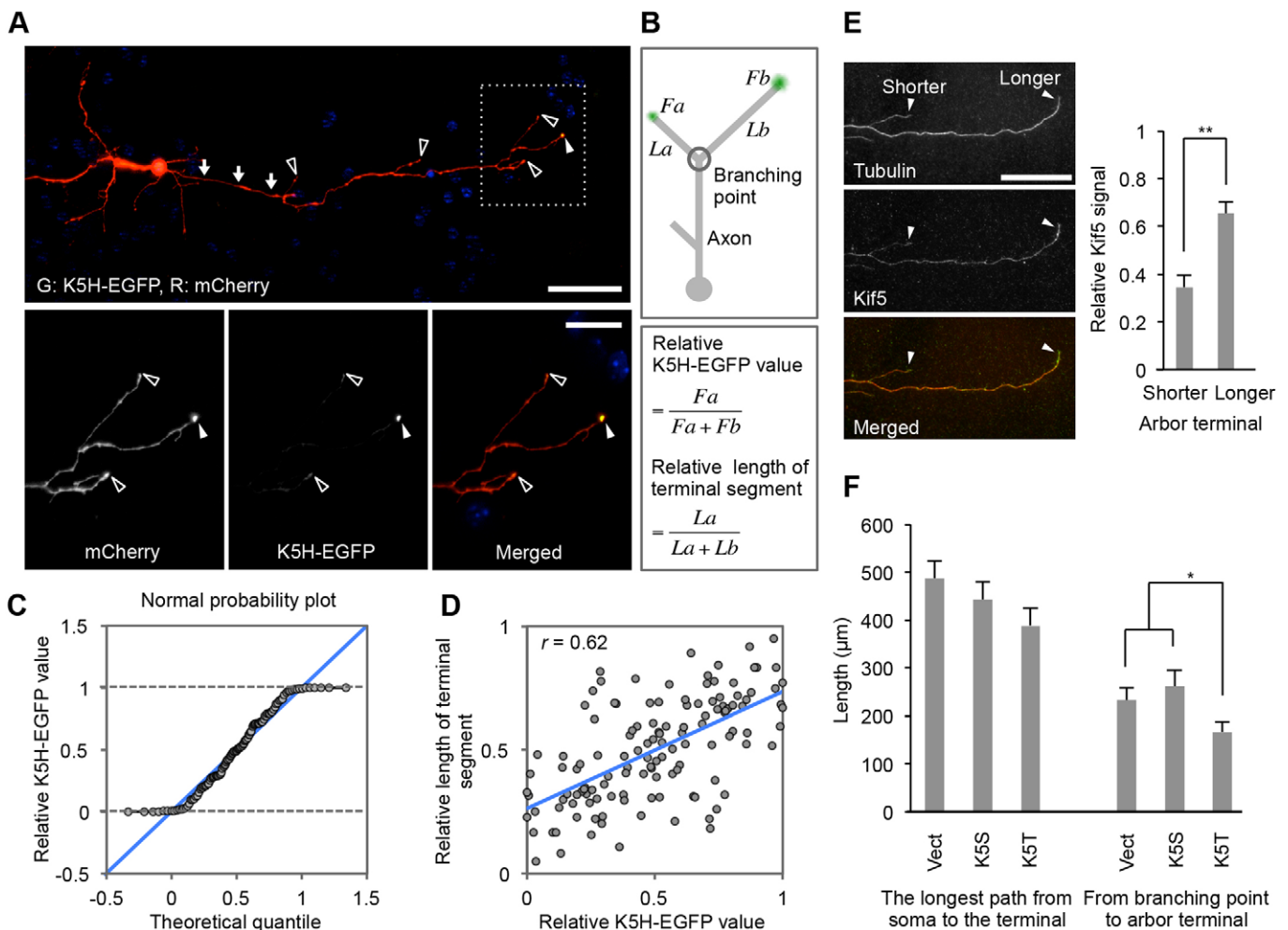


Fig. 1. The distribution of kinesin-1-mediated transport in axonal arbors. (A) CGNs that were transfected with plasmids for K5H-EGFP (green) and mCherry (red) were analyzed at 7 DIV. Magnified images of the axonal arbor (dotted box) are shown in the lower panels. K5H-EGFP is selectively transported in the axon (arrows) and accumulated at the end of one of the arbor terminals (filled arrowhead). In other terminals (open arrowheads), the K5H-EGFP signal was weak or undetectable. Scale bars: 50 μm (upper panel); 20 μm (lower panels). (B) Schematic representation of the data quantification of the K5H-EGFP signals and length of terminal segment. Terminal pairs (more than 20 μm the length) were selected for the analysis. Formulas for relative K5H-EGFP signal value as well as relative length of terminal segment are shown. (C) A quartile–quartile plot of the relative K5H-EGFP signal values versus theoretical quantiles. Note that the data plots do not align on a diagonal line. (D) A scatter plot of the relative length of the terminal segment versus the relative K5H-EGFP value. Moderate but significant positive correlation between two datasets was revealed ($r=0.62$, $P<0.001$, $n=64$). (E) A low-density culture of CGNs was stained with antibody against Kif5. The Kif5 signal value at axonal terminal is higher in longer terminal segments compared with shorter terminal segments (** $P<0.01$, $n=12$). Results are mean \pm s.e.m. ($n=12$). Scale bar: 50 μm . (F) Inhibition of axonal transport mediated by kinesin-1. CGNs were introduced with plasmid for the tail region of Kif5 (K5T), which disrupts the interaction with cargos, or the stalk region of Kif5 (K5S) as a control. Although the longest path from the soma to distal terminal end of axon tended to be shorter in K5T-expressing neurons, no significance was obtained in this analysis ($P=0.06$ and 0.29 compared with vector and K5S, respectively). The length from branching point on the longest path to axonal terminals in K5T-expressing neurons was significantly shorter than that of control neurons (* $P<0.05$). Results are mean \pm s.e.m. ($n=37$). P -values were calculated with a two-tailed Student's t -test.

extension of collateral branch can be observed (Fig. S1). In the current study, the analyses were carried out without distinguishing between the main axonal process and branches formed through collateralization or bifurcation.

CGNs introduced with an expression vector for K5H–EGFP (Kif5c head fused to EGFP) were fixed at 7 DIV. As previously described (Nakata and Hirokawa, 2003; Jacobson et al., 2006), K5H selectively accumulates in the axon terminals (Fig. 1A). The signal intensity of K5H in each terminal varied substantially, even in the same axonal arbor (Fig. 1A, arrowheads). To objectively evaluate K5H signal variation, signals at the distal terminal pairs were quantified and relative signal levels were calculated. Simultaneously, the relative length of terminal segment (from the branching point to the terminal end) was calculated as shown in Fig. 1B, and terminal segments were categorized merely based on the length. If K5H molecules are randomly delivered into two neighboring terminals, the distribution of relative signal values should follow a normal distribution. The quantile–quantile plot of sample quantiles of relative K5H values versus theoretical quantiles did not lie on a straight diagonal line, because some fractions revealed low (close to 0) or high (close to 1) relative K5H values (Fig. 1C), indicating that data were not normally distributed. The scatter plot of relative K5H values versus the relative length of the same terminal pair revealed a mild, but significant, positive correlation (Fig. 1D, $r=0.62$, $P<0.001$, $n=64$). These results indicate that K5H is preferentially delivered into a subset of arbor terminals that tend to be longer than neighboring terminals in the CGNs.

We also cultured CGNs at a low density (Kubota et al., 2013), and subjected the cells to immunocytochemistry (at 5 DIV) using antibodies specific to kinesin-1 (Fig. 1E) as previously described (Konishi and Setou, 2009). Results showed that endogenous kinesin-1 signals in longer terminal segments were greater than in shorter terminal segments (Fig. 1E, $P<0.01$, $n=12$), suggesting that results observed by using K5H represent, at least in part, the nature of endogenous kinesin-1-mediated axonal transport. In addition, when we disrupted kinesin-1-mediated axonal transport by expressing the cargo-binding (tail) domain (K5T), we found that the length from branching point to axonal terminal became shorter compared with control neurons introduced with empty vector or vector for stalk region (K5S) (Fig. 1F, $P<0.05$, $n=37$). These results support our notion that selective delivery of kinesin-1 in a subset of arbor terminals might coordinate the shape of axonal arbors by controlling the length of terminal segments.

Retraction is inhibited in axonal terminals with accumulated K5H

To determine whether kinesin-1-mediated transport efficiency in arbor terminals correlates with elongation or stability, we simultaneously observed changes in axonal morphology and K5H distribution within the axonal arbor by fluorescence time-lapse imaging. Although a majority of arbor terminals were stable, both growth and retraction occurred in a terminal-dependent manner at 5 DIV (Fig. 2A,B). K5H signals stably accumulated in a subset of arbor terminals in most cases, but signals occasionally changed location to the other terminals. The rate of terminal growth was determined by differentiating the length of the terminal segment at each time period. The values for elongation (i.e. positive growth) and retraction (i.e. negative growth) for each arbor terminal were then extracted. The scatter plot revealed that the average rate of elongation and retraction largely varied depending on the terminal

(Fig. 2C,D). Comparisons of the average elongation rate between terminals with a lower amount of K5H (i.e. relative K5H value <0.1 , $n=77$) and K5H-enriched terminals (i.e. relative K5H value >0.1 , $n=20$) revealed a significant median shift ($0.17 \mu\text{m/h}$ in low-K5H versus $0.75 \mu\text{m/h}$ in high-K5H terminals, $P<0.001$, Mann–Whitney *U*-test). Nevertheless, the relationship between K5H signal values and elongation rates remains unclear, because the a high rate of elongation frequently occurred even in K5H-deprived arbor terminals, and also was not remarkable in terminals that exhibited very high K5H signals (Fig. 2C). Additionally, some arbor terminals deprived of K5H exhibited no growth rate, because they were removed by retraction within a short period of time. Conversely, the average retraction rate was consistently low in K5H-enriched arbor terminals (Fig. 2D), with statistical significance differences in the median ($0.90 \mu\text{m/h}$ in lower K5H versus $0.57 \mu\text{m/h}$ in higher K5H, $P<0.05$, Mann–Whitney *U*-test). Consequently, although K5H-deprived terminal segments tended to become shorter, K5H-enriched terminal segments became longer or kept their length (Fig. 2E). Following these observations, we decided to focus our analysis on the relationship between the differential terminal retraction and efficiency of kinesin-1-mediated axonal transport in the arbor.

Local inhibition of kinesin-1-enhanced retraction rate of arbor terminals

We then applied chromophore-assisted light inactivation (CALI) to inhibit kinesin-1 activity in a terminal-dependent manner. KillerRed (KR) has been used as a genetically encoded photosensitizer for CALI (Destaing et al., 2010; Baumgart et al., 2012; Sano et al., 2014). To inhibit endogenous kinesin-1, CGNs were expressed with fusion protein consisting of KR and the kinesin light chain KLC1 (KR–KLC). KR–KLC fluorescence within a small circular area can be selectively bleached by illumination with a mercury lamp through the iris. An $\sim 60\%$ and $\sim 80\%$ loss of KR–KLC signal was observed within 30 s and 60 s of exposure, respectively (Fig. 3A,B). At the axonal terminal segment, KR and KR–KLC were distributed throughout the process (Fig. 3C,D). Unlike K5H, it is expected that KR–KLC proteins exist in various states (e.g. as free forms and as a kinesin complex binding to various type of cargos). We illuminated the axonal terminal and monitored fluorescence recovery. Recovery of the KR signal reached a maximum in the first time-point analyzed (15 min) after bleaching, at which time half of signal relative to the pre-illumination was detected, and subsequently decayed (Fig. 3C,E). In addition, a reduction in the KR signal was observed even outside of the illuminated area. We conclude that a part of signal was lost during the photobleaching and subsequent imaging, and fast recovery of KR represents fast diffusion of free KR proteins. By contrast, recovery of KR–KLC at 15 min was smaller compared than recovery of KR, then slowly increased and reached a similar level at 3 h (Fig. 3D,E).

We applied CALI to one side (longer terminal segment) of a terminal pairs of neurons expressing KR or KR–KLC together with EGFP. Subsequently, the effect of CALI application on the arbor terminals was examined by monitoring EGFP signals for 8 h (Fig. 3F; Fig. S2). Given that in a preliminary experiment, 60 s of illumination caused immortalization or disintegration of arbor terminal, we applied 30 s of exposure in this analysis to reduce photo toxicity. We measured the difference in length of both the target terminal segment and the neighboring un-illuminated terminal segment at 15-min and intervals of 15 min thereafter. Most arbor terminals exhibited a limited retraction after CALI exposure in KR-expressing CGNs, whereas in KR–KLC-expressing

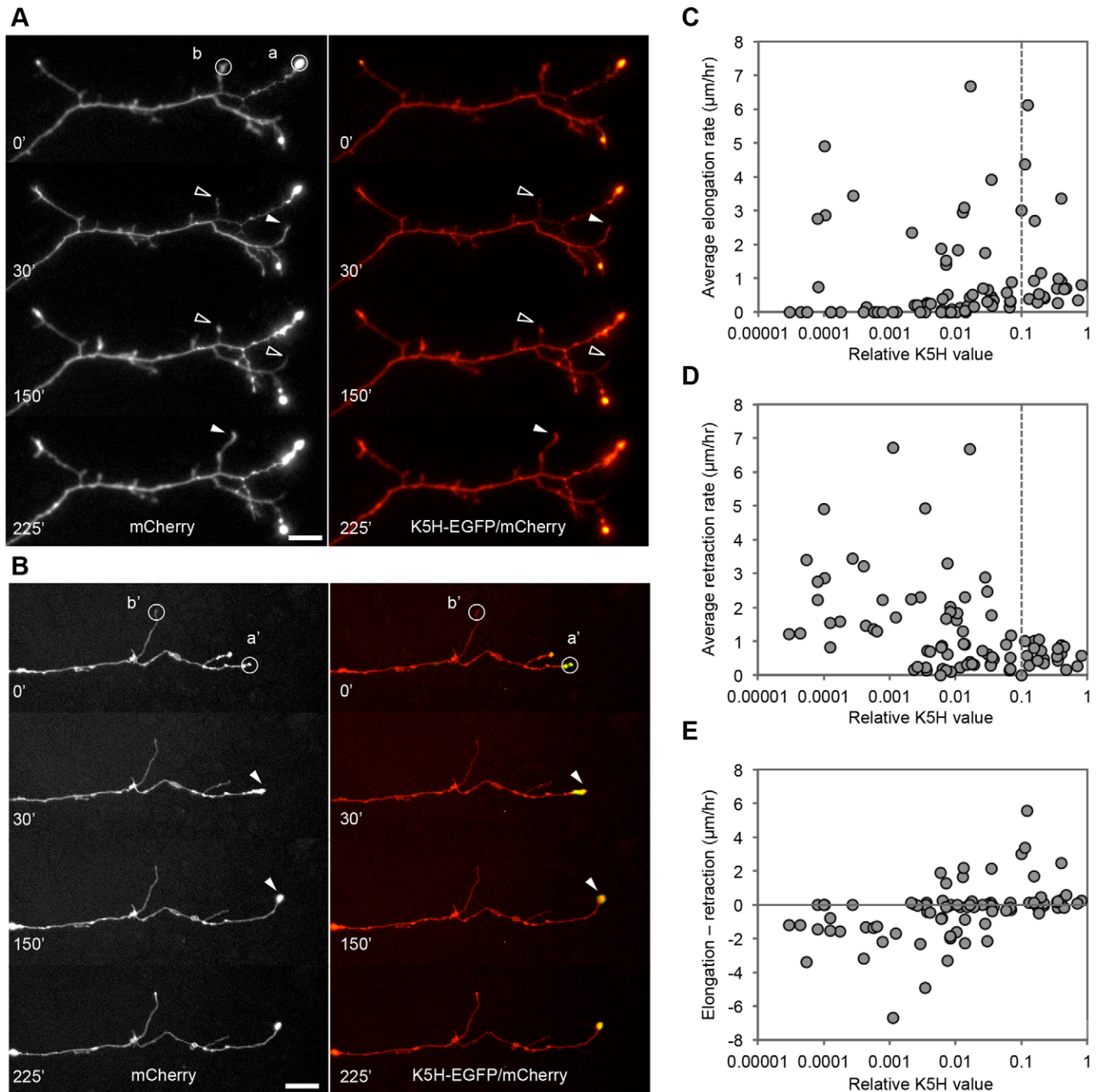


Fig. 2. Time-lapse imaging of K5H distribution and axonal arborization. (A,B) CGNs that were transfected with plasmids for K5H-EGFP (green) and mCherry (red) were subjected to the time-lapse imaging analysis at 5 DIV. Images were taken every 15 min overnight, and individual images taken at the indicated time obtained from two different neurons are shown. Examples of arbor terminals that possess relatively high (a,a') or low (b,b') K5H signal are marked. Elongation and retraction of arbor terminals is indicated by filled and open arrowheads, respectively. (C,D) Scatter plots of average elongation rate of arbor terminal versus relative K5H-EGFP value (C), and average retraction rate of arbor terminal versus relative K5H-EGFP value (D). The relative K5H-EGFP level in each terminal was determined by calculating the ratio of the signal at the terminal to the total signal value in the axonal arbor, and an average value within the time window subjected to the analysis was calculated. For terminals that only existed for a certain period, an average value for that period was calculated. Data were collected from 97 arbor terminals in multiple neurons. Each circle in the plots represents an individual arbor terminal. For statistical analysis, datasets were separated into two groups (i.e. relative K5H value <0.1 , $n=77$, and relative K5H value >0.1 , $n=20$). A significant median shift was detected for both elongation and retraction (elongation, $P<0.001$; retraction, $P<0.05$, Mann-Whitney U -test). (E) Scatter plot of average difference in length (i.e. elongation rate - retraction rate) versus relative K5H-EGFP value. Scale bars: 50 μm .

CGNs, intermittent retraction was only observed at the arbor terminal exposed to CALI (target terminal) (Fig. 3F; Fig. S2). Although there was no clear time window that the boost of retraction occurred, retraction was not remarkable in the last few hours of the

analysis (Fig. S2). Given that the KR-KLC signal recovered to a similar level to that of KR in 3 h after photobleaching, we calculated the amount of retraction in 3 h (Fig. 3G). Quantification of terminal retraction values revealed greater retraction in KR-KLC-expressing

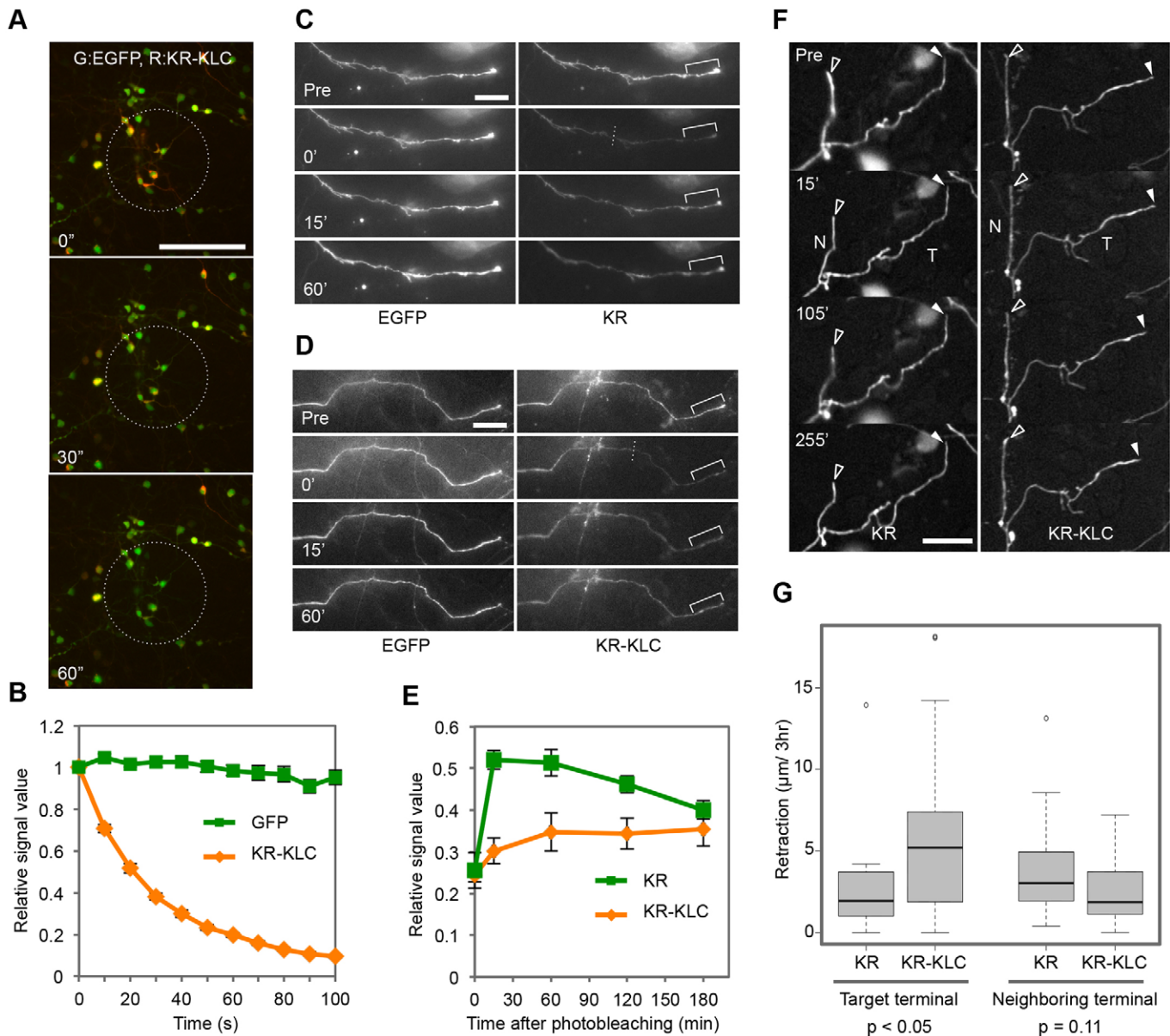


Fig. 3. CALI-mediated local inhibition of kinesin-1 in the arbor terminal. (A) Region-dependent photobleaching of KR–KLC. CGNs expressing KR–KLC (red) and EGFP (green) were subjected to photobleaching within the indicated circular area. Images taken before (0 s) and 30 s and 60 s after photobleaching are shown. Scale bar: 100 μm. (B) Signals for KR–KLC and EGFP in the soma of CGNs during photobleaching (mean±s.e.m., $n=6$). Fluorescence of KR–KLC, but not EGFP is rapidly decreased by illumination. (C,D) Distribution and recovery after photobleaching of KR and KR–KLC signals at the axonal terminal. CGNs expressing KR (C) or KR–KLC (D) were subjected to photobleaching at the axonal terminal. A region of ~50 μm in diameter from the terminal (the dotted line indicates the approximate position of the border) was illuminated for 60 s, and recovery of signals within 20 μm of the terminal (bracket) was monitored at the indicated time. Scale bar: 20 μm. (E) Quantified (mean±s.e.m.) results of fluorescence recovery of KR (green; $n=6$) and KR–KLC (orange; $n=5$) in axonal terminals. The signal value was normalized to the EGFP signals. Fluorescence recovery of KR–KLC was slower than that of KR. At 3 h after photobleaching, KR and KR–KLC signals became a similar level. (F, G) CALI analysis on arbor terminal pairs expressing KR (left) and KR–KLC (right). Representative arbor terminals before (Pre) and after CALI at the indicated time (F). Arbor morphology was visualized with EGFP signals. The longer terminal that received CALI (target terminal; T) and the shorter unilluminated terminal (Neighboring terminal; N) are indicated (F). Filled and open arrowheads indicate the arbor terminal for each segment. Values of retraction at 3 h after CALI were quantified and presented in box plot with outliers (open circles). The box represents the 25–75th percentiles, and the median is indicated. The whiskers show the smallest and largest values within a distance of 1.5× interquartile range above and below the limits of the box. (G). P -values at the bottom indicate the results of statistical analysis (Mann–Whitney U -test) between the axonal terminals expressing KR ($n=19$) and KR–KLC ($n=18$). Scale bars: 20 μm.

CGNs ($n=18$) compared with KR-expressing control neurons ($n=19$) at target terminals (Fig. 3G, $P<0.05$, Mann–Whitney U -test). In contrast, retraction of the neighboring shorter terminal segment that did not receive photo illumination (neighboring terminal) was not greater in KR–KLC-expressing CGNs than in control neurons ($P=0.11$).

Microtubule turnover is differentially regulated between neighboring terminal segments

To determine whether K5H accumulation in a subset of axonal terminals reflects a variation in microtubule content between terminal segments, we expressed mCherry–tubulin and K5H–EGFP in CGNs because introduction of the K5H–EGFP plasmid

requires a high-density culture, which makes it difficult to detect endogenous tubulin in a single axonal arbor by immunocytochemistry. In order to estimate the amount of microtubules with this method, signals from mCherry–tubulin that is incorporated in microtubules have to be separated from those of free mCherry–tubulin. To remove unpolymerized free tubulin, neurons were subjected to simultaneous extraction and fixation at 7 DIV (Fig. 4A). Signals at the terminal pairs were quantified, and relative signal levels were calculated (Fig. 4B). In some of the terminal pairs, the longer terminal segment enriched with K5H exhibited greater mCherry–tubulin signals (Fig. 4A). However, in other terminal pairs, greater K5H accumulation was observed in terminal segments with less mCherry–tubulin (Fig. 4A). Consequently, the overall correlation between K5H–EGFP values and mCherry–tubulin signals in the same terminal pair was not significant (Fig. 4B, $r=0.30$, $P=0.33$, $n=44$). These results indicate that factors other than microtubule content might contribute to the preferential accumulation of K5H in longer terminal segments.

Previous studies focused on neuronal polarity have suggested that kinesin-1 is preferentially transported in processes that contain acetylated and detyrosinated microtubules (Reed et al., 2006; Konishi and Setou, 2009; Hammond et al., 2010). Stable microtubules contain more detyrosinated and acetylated tubulins than dynamic microtubules (Janke and Bulinski, 2011). Therefore, we analyzed microtubule turnover in axonal arbors. We applied fluorescence recovery after photobleaching (FRAP) by expressing an α -tubulin tagged with EGFP (EGFP–tubulin). In CGNs, EGFP–tubulin was detected throughout axonal arbors (Fig. 4C). We focused on pairs of arbor terminals and applied photobleaching in a rectangular area proximal (approximately 10 μm) to the branching point (Fig. 4C). Recovery of fluorescence in each terminal segment was measured at 40-s intervals. Because free tubulins are rapidly recovered in a matter of seconds, fluorescence recovery over time reflects mostly the turnover of EGFP–tubulins that exist as microtubules. Notably, when FRAP analysis was applied on terminal segments that possessed varying segment lengths, we

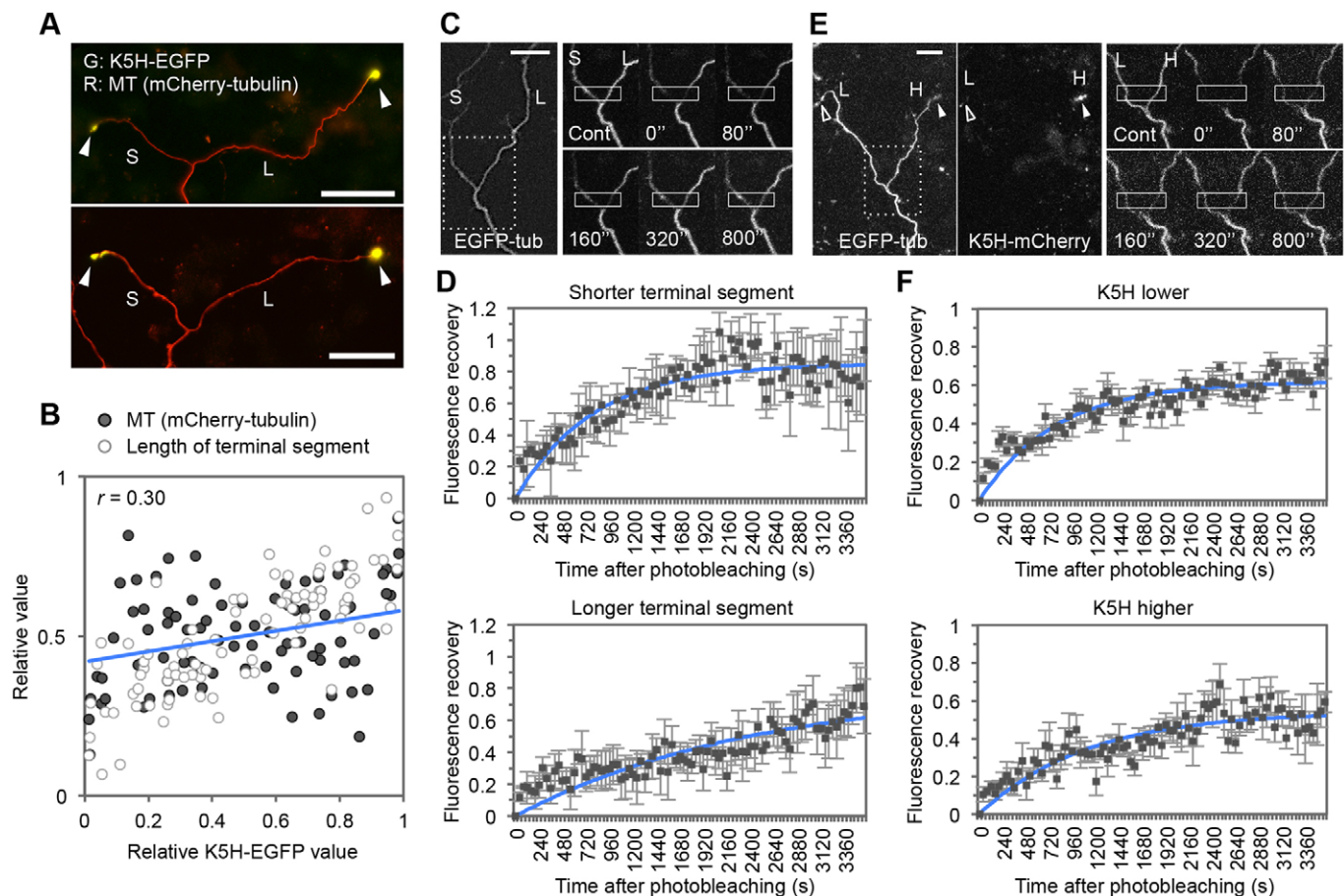


Fig. 4. Analysis of microtubule differences in neighboring terminal segments. (A) Neurons at 7 DIV that have been transfected with plasmid for mCherry–tubulin (red) and K5H–EGFP (green) were simultaneously fixed and permeabilized to remove unpolymerized mCherry–tubulin. Two representative terminal pairs possessing shorter (S) and longer (L) terminal segments are shown. The arrowheads mark the terminal ends. Scale bars: 50 μm . (B) Scatter plot of relative mCherry–tubulin value versus relative K5H–EGFP value (filled circles). Only a small correlation between two datasets was observed ($r=0.30$, $P=0.33$, $n=44$). The plot for relative length of terminal segment versus relative K5H–EGFP value is also shown (open circles) as in Fig. 1D. MT, microtubules. (C) Neurons were transfected with plasmid for EGFP–tubulin, and microtubule turnover in the pairs of terminal segments that were different in length (>twofold) were analyzed by FRAP. The photobleached region (about 10 μm distal from the branching point) across the shorter (S) and longer (L) terminal segments is indicated by rectangles. The recovery was monitored every 40 s. (D) Quantified results of fluorescence recovery of EGFP–tubulin in axonal terminals (mean \pm s.e.m., $n=6$). Fluorescence recovery of EGFP–tubulin is faster in shorter terminal segments (upper) compared with longer terminal segments (lower) (data obtained from four experiments are shown). (E) Neurons were transfected with plasmids for EGFP–tubulin and K5H–mCherry, and pairs of terminal segments that had a comparable length (<1.5-fold difference) were subjected to FRAP as in C. A pair of axonal terminals expressing a low (L) and high (H) amount of K5H is shown. (F) The fluorescence recovery of EGFP–tubulin in terminal pairs that have similar segment length but show a difference in K5H signals (mean \pm s.e.m., >twofold, $n=6$). Scale bars: 20 μm .

found that recovery of EGFP–tubulin in longer axonal terminal segments was slower than in shorter ones (Fig. 4D). The dissociation rate of EGFP–tubulin, which was obtained by a mathematical fitting to the model (Edson et al., 1993; Hush et al., 1994; see Materials and Methods), revealed that turnover of EGFP–tubulin was slower in longer terminal segments compared with shorter terminal segments (Fig. S3A, shorter terminal segment; $k_{off}=0.055\pm 0.019/\text{min}$ versus longer terminal segment; $k_{off}=0.017\pm 0.006/\text{min}$, mean \pm s.e.m., $n=4$).

We also assessed the possibility that selective kinesin-1 transport directly correlates with microtubule stability in the terminal segments. In this experiment, FRAP was applied to CGN axons that simultaneously expressed EGFP–tubulin and K5H–mCherry. As described above, the length of the K5H-enriched terminals tended to be longer than neighboring terminal segments (Fig. 1D). To investigate the direct correlation between K5H signal and turnover of EGFP–tubulin, we selected terminal pairs that were comparable in segment length (<1.5-fold difference). When we analyzed terminal pairs that possessed different amounts of K5H (>2-fold), we found no significant correlation between EGFP–tubulin recovery and K5H signal value (Fig. 4E,F). In addition, no significant correlation was observed between the K5H signal value and the dissociation rate of EGFP–tubulin (Fig. S3B).

Correlation between length of terminal segment and reporters of microtubule stability

We next performed immunocytochemistry by using antibodies that specifically recognize post-transcriptionally modified tubulins (Fig. 5A). The ratios of tyrosinated to detyrosinated tubulins and acetylated tubulins varied between neighboring terminal segments with different lengths. Consistent with a previous report (Robson and Burgoyne, 1989; Ahmad et al., 1993; Brown et al., 1993), the ratio of modification gradually changed depending on the distance from the branching point (Fig. 5A). To account for region-dependent differences in tubulin modification within the terminal segment, we quantified staining profiles for distances from axonal branching points and distances from terminal ends (Fig. 5B,C). Notably, the ratio of tyrosinated to detyrosinated tubulin was greater in shorter terminal segments compared with longer terminal segments at the same distance from a branching point. The ratio difference increased in a distance-dependent manner, but was significant even at 10 μm from the branching point (Fig. 5C, $P<0.05$, $n=11$). These results were consistent with the FRAP analysis. Similarly, the ratio of acetylated tubulin in shorter terminal segments was significantly less than the ratio at the same position in longer terminal segments relative to the branching point (Fig. 5C, $P<0.05$ at 10 μm , $n=8$). Conversely, in both tyrosination and detyrosination and acetylation, staining profiles versus distance from terminal ends were similar between shorter and longer terminal segments (Fig. 5C).

We further investigated the region-dependent frequency of microtubule growth in the arbor by introducing an end-binding 3 (EB3, also known as MAPRE3) plasmid that was fused to fluorescent proteins to label plus-ends of growing microtubules (Stepanova et al., 2003). EB3 particles were detected more frequently in distal regions compared with proximal regions, and shorter terminal segments contained more particles compared with longer terminal segments at the same distance from a branching point (Fig. 5D, $P<0.05$, $n=9$). Additionally, profiles of EB3 particle numbers versus distance from terminal ends were similar between shorter and longer terminal segments (Fig. 5D), which was consistent with analysis of tyrosination and detyrosination and acetylation of microtubules. Thus, differences in microtubule

turnover between short and long terminal segments could be explained by a regional difference that is dependent on the distance from a terminal end. In a previous study, Seetapun and Odde (2010) provided a simple length-dependent model for selective accumulation of stable microtubules in axons during polarization, which does not require neurite-dependent control of a microtubule assembly. In this model, the growth rate of microtubules in minor and longer processes remained unaltered. However, because the traveling time depends on process length, the net turnover of microtubules is slower in longer processes (i.e. axons) compared with shorter minor processes. We measured microtubule growth in axonal arbors by simultaneously monitoring EB3 particles in shorter and longer terminal segments (Fig. 5E). We found no length-dependent difference in the velocity of EB3 particles (Fig. 5E). These results support the notion that microtubule turnover in terminal segments is differentially regulated and dependent on distance from the terminal end, rather than by segment-specific microtubule regulation.

F-actin distribution in the axonal arbor spatiotemporally correlates with K5H

We next investigated the relationship between F-actin and K5H at arbor terminals. F-actin accumulates in the growth cone and is required to form filopodia and lamellipodia (Lewis et al., 2013). In axons of young CGNs (at 2 DIV), strong F-actin signals were observed in the growth cone by staining with phalloidin. However, at 5 DIV, a time point by which axons have become thinner and form multiple terminals, F-actin signals at the axonal tip were highly restricted (Fig. S4A). To analyze F-actin distribution in detail in CGN axons, we expressed Lifeact, a marker for the visualization of F-actin (Riedl et al., 2008). In the axonal arbor, Lifeact signals colocalized with phalloidin signals at arbor terminals and protrusions (Fig. S4B). When we simultaneously expressed K5H and Lifeact in neurons, they colocalized in the axonal terminal (Fig. 6A). Plotting of relative Lifeact signal values versus relative K5H signals in terminal pairs clearly revealed a positive correlation (Fig. 6B, $r=0.83$, $n=20$). Consequently, arbor terminals with greater K5H local levels also had significantly greater Lifeact signals (Fig. 6B, $P<0.001$, $n=15$). To analyze the temporal correlation, axonal arbors expressing K5H and Lifeact were subjected to time-lapse imaging analysis at 10-min intervals. In some arbor terminals, the K5H signal dramatically decreased or increased during the time-lapse period (Fig. 6C). In these arbor terminals, K5H signal changes were followed by changes in Lifeact signal values (Fig. 6C,D). We collected data from arbor terminals in which the K5H signal changed >twofold within 100 min. When the Lifeact signals between the two different time points (i.e. maximum K5H versus minimum K5H) were compared, we found a significant difference (Fig. 6D, $P<0.001$, $n=5$). These results suggested a spatiotemporal correlation between the K5H and Lifeact signals.

To determine whether F-actin regulation plays a role in the retraction that frequently occurs in K5H-deprived arbor terminals, we utilized Latrunculin A, which has been shown to inhibit axonal retraction in sensory neurons by disrupting actin polymerization (Ahmad et al., 2000; Gallo et al., 2002). Neurons that express K5H–EGFP and mCherry were treated with Latrunculin A prior to time-lapse imaging. Changes in axonal morphology and distribution of K5H–EGFP were simultaneously analyzed for 5 h to determine the primary effect of inhibiting actin turnover. We observed that Latrunculin A-treated arbor terminals ($n=21$) exhibited a lower average retraction rate compared with vehicle-treated control arbor terminals ($n=26$) (Fig. 6E, median; 0.80 $\mu\text{m}/\text{h}$ in DMSO versus

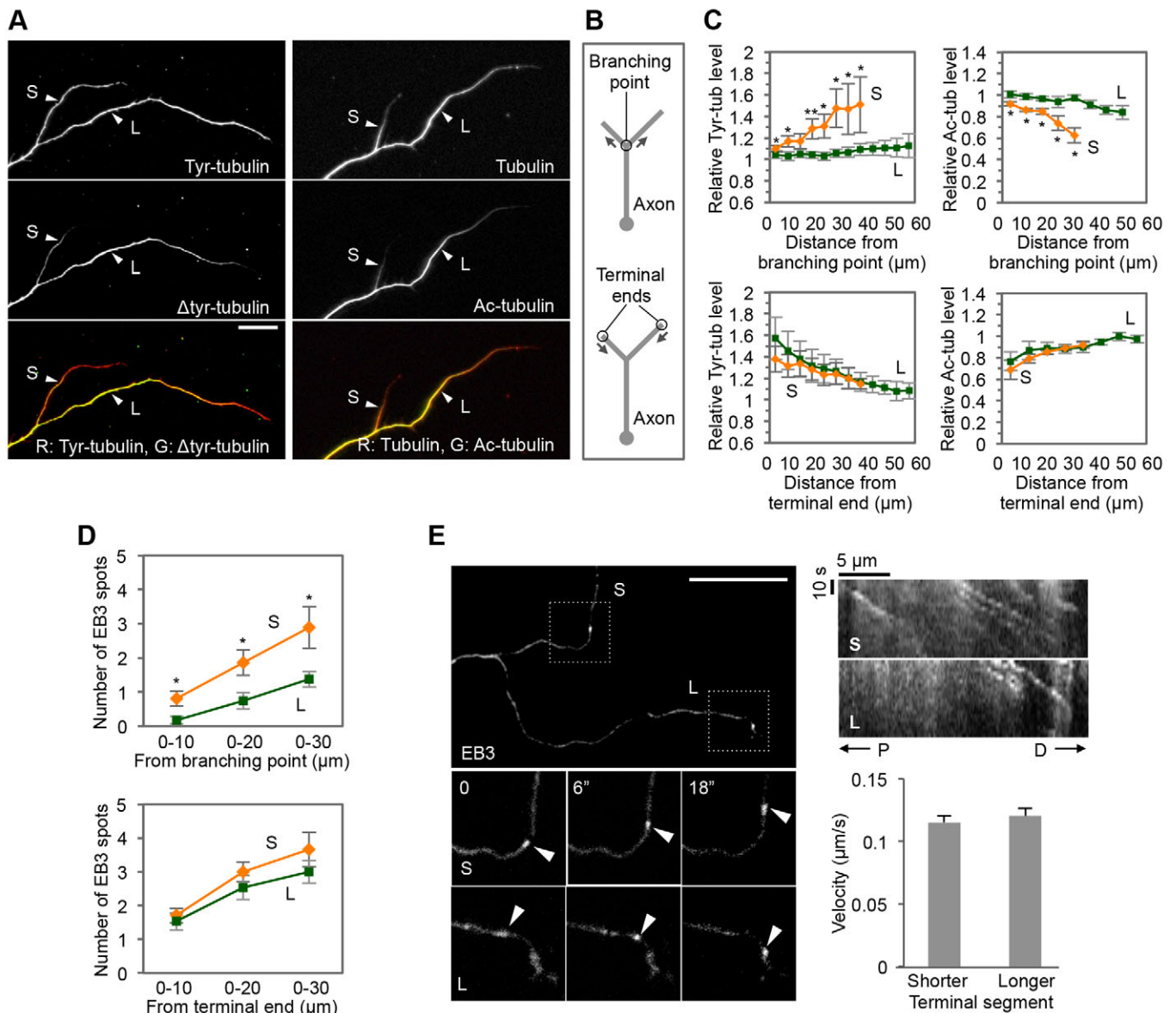


Fig. 5. Regulation of microtubules depends on the length of terminal segment in axonal arbors. (A) Distribution of tyrosinated (Tyr) and detyrosinated (Δ Tyr) tubulins as well as acetylated (Ac) tubulins in CGN axonal arbors detected by immunocytochemistry. Shorter (S) and longer (L) axonal terminal segments are indicated (arrowheads). Scale bar: 20 μ m. (B) Schematic representations of the data quantification for the analysis of region-dependent tubulin modification. The signal profiles for the distance from the branching point or distance from the terminal ends were calculated. (C) Quantification (mean \pm s.e.m.) of the region-dependent tyrosination and acetylation on the tubulins in shorter (S; orange) and longer (L; green) terminal segments. The tyrosinated tubulin (Tyr-tub) level was determined by taking the ratio of the amount of tyrosinated and detyrosinated tubulin, whereas acetylated tubulin (Ac-tub) level is indicated by the ratio to the tubulin signal. The Tyr-tub and Ac-tub level in each region was normalized to the signal at the branching point (Tyr, $n=11$; Ac, $n=8$). (D) The EB3-expressing neurons were fixed with methanol, and the number of EB3 particles in every 10 μ m on the terminal segment was measured. The number of EB3 particles versus the distance from branching point (upper) as well as the distance from terminal end (lower) is presented ($n\geq 9$). Graphs represent mean \pm s.e.m. (E) CGNs expressing EB3 that was fused to fluorescent protein were subjected to time-lapse imaging. Data were acquired from arbor terminal pairs that had a difference in segment length (>twofold). Scale bar: 20 μ m. Magnified images of EB3 particles (dashed squares) are shown at the bottom. Representative kymographs for shorter (S) and longer (L) terminal segments are shown at the top right (P, proximal; D, distal). The graph (bottom right) represents velocity of EB3 particles calculated from kymographs (mean \pm s.e.m., $n\geq 31$).

0.49 μ m/h Latrunculin A, $P<0.05$, Mann–Whitney U -test). Taken together, these results indicate the possibility that actin-dependent mechanisms are involved in the axonal retraction that occurs in kinesin-1-deprived arbor terminals.

DISCUSSION

The intracellular systems involved in how neurons differentially regulate growth and stability of arbor terminals within the same

axon remain largely unknown. Previous results have indicated that intracellular Ca^{2+} mediates the competitive signal between different terminals of the same axon (Hutchins and Kalil, 2008). However, the mechanisms by which localized Ca^{2+} signals regulate the axonal structure in a region-specific manner remain to be elucidated. Other molecules that are differentially controlled between axonal terminals need to be identified. In this study, we found that K5H tagged by fluorescent protein, as well as endogenous kinesin-1,

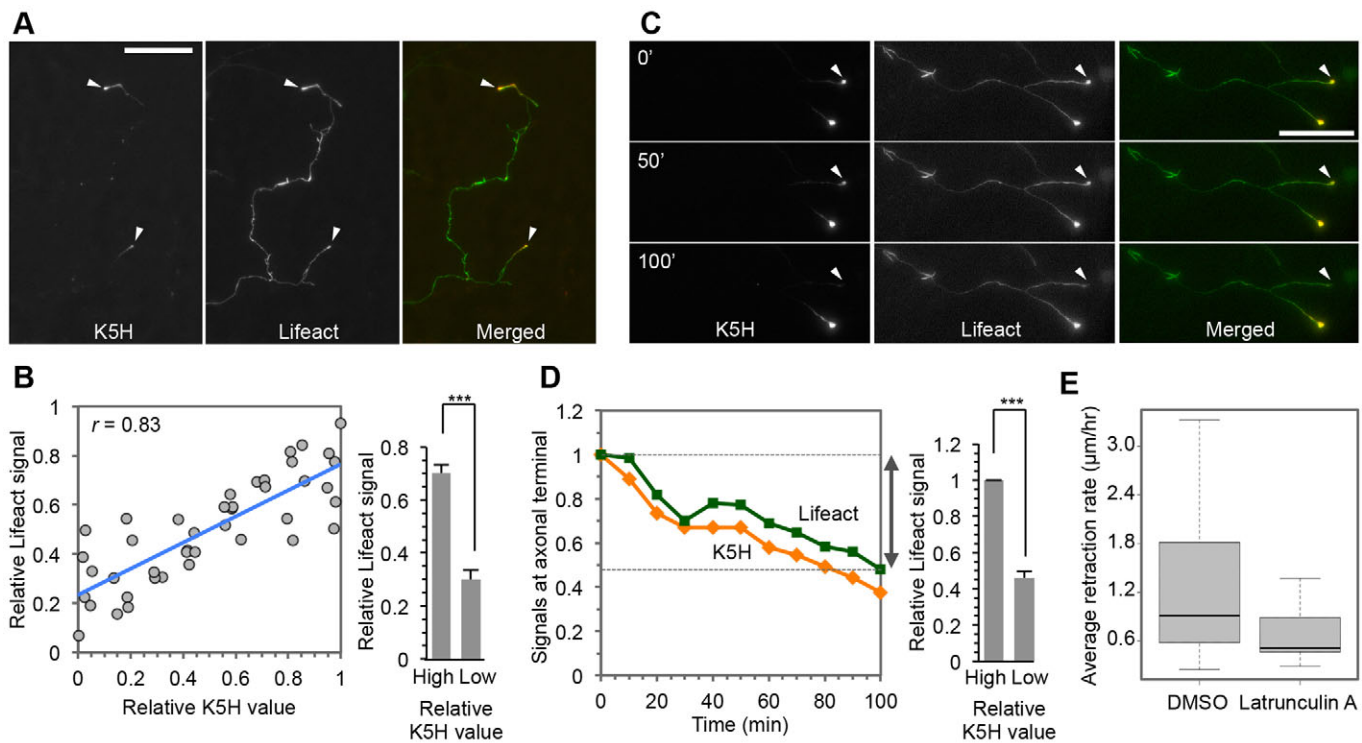


Fig. 6. Distribution of F-actin in axonal terminals of CGNs. (A) Axonal arbor of a CGN that expresses Lifeact and K5H. (B) Scatter plots of Lifeact signal values at axonal terminal versus K5H signals reveals positive correlation (left; $r = 0.83$, $n = 20$). The Lifeact signal is significantly higher in the axonal terminals that contain a higher K5H signal compared with the axonal terminals that contain lower K5H signals (right; mean \pm s.e.m., $n = 15$). *** $P < 0.001$ (two-tailed Student's t -test). (C) Simultaneous alternation of K5H and Lifeact distribution in axonal terminals of living neurons. Representative images of an axonal arbor in which K5H signal was changed substantially (arrowheads) during imaging are shown. (D) Quantified result of the time-lapse imaging shown in C. Imaging data from five different axonal arbors were subjected to statistical analysis (right). Data are mean \pm s.e.m. and are collected from axonal terminals in which a >twofold change in K5H signal occurred during the time-lapse imaging (100 min) ($n = 5$). *** $P < 0.001$ (two-tailed Student's t -test). (E) Inhibition of actin turnover disrupts the retraction of axonal terminals. CGNs that had been transfected with vectors for mCherry and K5H-EGFP were treated with 1 μM Latrunculin A or DMSO, followed by time-lapse imaging. Average retraction rate of axonal terminals were measured as in Fig. 2, and shown in a box plot. The box represents the 25–75th percentiles, and the median is indicated. The whiskers show the smallest and largest values. Latrunculin A treatment inhibited the retraction of axonal terminals ($P < 0.05$, DMSO; $n = 26$, Latrunculin A; $n = 21$, Mann–Whitney U -test). Scale bars: 50 μm .

accumulate in a subset of axonal arbor terminals (Fig. 1). The quartile–quartile plot analysis of K5H signals in axonal terminals revealed that the differences in K5H signals between terminals are not due to random variation. We only analyzed terminal segments that had a length $>20 \mu\text{m}$ to avoid collecting data from newly formed protrusions that had not yet been invaded by microtubules (Gallo, 2011). Furthermore, time-lapse imaging revealed that K5H signals occasionally and rapidly changed their distribution, but that local levels of K5H did not increase in the subset of axonal terminals that exhibited a long lifespan. These findings revealed selective sorting of kinesin-1 in the axonal arbor. Time-lapse imaging analysis revealed that axonal terminals with high local levels of K5H exhibited a small retraction (Fig. 2). Consistently, local inhibition of kinesin-1 by CALI enhanced retraction specifically at the illuminated axonal terminal (Fig. 3). Considering the function of kinesin-1-mediated axonal transport, the accumulation of cargo molecules in particular axonal terminals would be expected to result in the deprivation of molecules in neighboring terminals. Results from the present study suggest a potential intracellular system for competitive stabilization of axonal terminals via kinesin-1 sorting in the axonal arbor. Additionally, changes in the length of terminal segment could provide feedback to kinesin-1-dependent transport as described below.

The mechanisms by which kinesin-1 gets sorted into a subset of axonal terminals from the axon remain to be clarified. Our results

showed that microtubules in longer terminal segments are more stable than those in neighboring shorter terminal segments when compared in the area proximal to the branching point (Fig. 4). Consistently, posttranslational modifications of tubulins abundant in stable microtubules (i.e. detyrosination and acetylation) are greater in longer axonal terminal segments (Fig. 5). Thus, kinesin-1-dependent terminal selection could be explained by preferential recruitment to stable microtubules as described in other paradigms (Reed et al., 2006; Hammond et al., 2010; Dunn et al., 2008). In a previous study, we have reported that inhibition of tubulin tyrosination in immature hippocampal neurons disrupts polarized K5H transport into axons (Konishi and Setou, 2009). We also found that inhibition of tubulin tyrosination by siRNA for tubulin tyrosination ligase (TTL) tended to inhibit the terminal-dependent accumulation of K5H in CGNs, although no statistical significance was obtained (data not shown). Thus, the function of tyrosination–detyrosination alone might be limited in this paradigm. It is possible that other differences (e.g. MAPs, GTP- or GTP-binding state, microtubule numbers) could also contribute to this process, because they are possibly affected by microtubule dynamics. Studies focused on neural polarity have shown the contribution of multiple factors that can be differentially coordinated dependent on the situation and neuronal types (Barnes and Polleux, 2009). Further studies are required to fully demonstrate the molecular mechanisms of kinesin-1 sorting in the axonal arbor.

Microtubules undergo repetitive growth and shortening until they reach the axonal terminal, where most microtubules undergo shrinkage (catastrophe). According to the polarization model by Seetapun and Odde (2010), because of increased traveling time from the soma, microtubule turnover is slower in the axon due to process length. Under certain conditions, the region closer to the terminal contains a larger number of growing microtubule plus-ends than regions further from the terminal. Consequently, the longer process contains older microtubules than shorter minor processes. Although microtubules in mature axons are segmented (Yu and Baas, 1994), our observations suggest that this model can be adopted to explain microtubule difference in axonal arbors. First, there is a positive correlation between the length of the terminal segment and microtubule turnover. Second, the distribution of reporters for microtubule turnover depends on distance from terminal end. Third, there is no segment-dependent difference in velocity of EB3 particles. Obviously, other factors could also regulate microtubules, either stochastically or in a region-specific manner through cleavage or stabilization (Yu et al., 2008; Homma et al., 2003; Peris et al., 2009). Indeed, we found only a moderate correlation between K5H signals and length of terminal segment, and K5H distribution can be suddenly altered prior to a change in length of terminal segment. These factors might play crucial roles in switching between a stable and unstable state in arbor terminals.

As described above, longer terminal segments contain more stable microtubules and tend to contain greater K5H signals. Previous studies have reported that kinesin-1 transports molecules involved in the stabilization of microtubules (Kimura et al., 2005). However, microtubule turnover in terminal pairs with comparable segment lengths, but differences in K5H signals, was not remarkably different. This observation contradicts the notion that kinesin-1-dependent inhibition of retraction is mediated by selective stabilization of microtubules. Conversely, there was a spatiotemporal correlation between K5H and F-actin signals in arbor terminals, and disruption of axonal turnover with Latrunculin A significantly inhibited retraction (Fig. 6), even in arbor terminals with low K5H signals. Actin regulation has been shown to play an important role in axonal growth, as well as retraction (Giannone et al., 2009). Retraction cues induce growth cone collapse by destabilizing F-actin in the axonal terminal. Conversely, RhoA- and myosin-II-driven contractility along intra-axonal F-actin mediates axonal retraction (Gallo et al., 2002; Gallo, 2006). Therefore, reorganization of F-actin is crucial for the retracting axon to change its structure. Although detailed molecular mechanisms remain to be elucidated, our current study raised a possible link between the differential control of terminal stability and actomyosin-mediated axonal retraction.

MATERIALS AND METHODS

Cell culture

Dissociated CGN culture was prepared according to the previous study (Konishi et al., 2004) with modifications. In brief, cerebella isolated from Slc:ICR mice (postnatal days 5–6) were digested with trypsin, and dissociated neurons were placed in Basal Medium Eagle (BME; Sigma-Aldrich, St Louis, MO) supplemented with 10% calf serum (Thermo Fisher Scientific, Waltham, MA), 1 mg/ml penicillin, 1 mg/ml streptomycin, 2 mM glutamine and 25 mM KCl. Neurons were spread on a plate that has been coated with poly-L-ornithine (Sigma-Aldrich). Low-density CGN cultures were prepared by co-cultivating with high-density CGN culture as described previously (Kubota et al., 2013). Animals were treated according to the institutional ethical guidelines of University of Fukui.

Transfection

Plasmid DNAs were introduced in CGNs by the calcium phosphate method. Prior to the transfection, CGN culture was washed twice with Dulbecco's modified Eagle's medium (DMEM; Sigma-Aldrich), then placed in DMEM and incubated at 37°C in a CO₂ chamber. DNA solution containing 250 mM CaCl₂, was gradually mixed with same amount of 2× HBS solution (270 mM NaCl, 9.5 mM KCl, 1.4 mM NaH₂PO₄, 15 mM glucose, 42 mM Hepes). After 15 min, the DNA mixture was added to cells and the cells were incubated for 15 min in CO₂ incubator. Finally, the CGN culture was washed twice with DMEM and placed in original medium. In the case of low-density culture, dissociated neurons were placed in DMEM that contained plasmids, and exposed to the square electric pulses (140 V, 5 ms for two times) before plating as described previously (Kubota et al., 2013). To construct a plasmid for KR–KLC, full-length *KLC1* cDNA was amplified by PCR, and inserted into pKillerRed-C vector (Evrogen, Moscow, Russia). Plasmids for EGFP–tubulin (#30487, gift from Tso-Pang Yao), mCherry–tubulin (#26768, gift from Torsten Wittmann), tdTomato–EB3 (#58090, gift from Michael Davidson) and pLifeAct–mTurquoise2 (#36201, gift from Dorus Gadella), were obtained from Addgene. Plasmids for EGFP–EB3, K5H–EGFP and dominant-negative Kif5s were as described previously (Konishi and Setou, 2009; Okamoto et al., 2015). K5H–mCherry was constructed by inserting the K5H sequence into pmCherry-N vector (BD Biosciences, Franklin Lakes, NJ). To knockdown TTL, a stealth siRNA against TTL (#RSS301756, Thermo Fisher Scientific) were transfected into CGNs together with plasmids for K5H–EGFP and mCherry by the calcium phosphate method as described above.

Immunocytochemistry

For immunocytochemistry, neurons were fixed for 15 min at room temperature with paraformaldehyde solution (4% paraformaldehyde in PBS) followed by permeabilization with 0.2–0.4% Triton X-100 in PBS for 15 min, and incubated further (1 h) with blocking solution (5% goat serum, 3% BSA and 0.02% Tween 20 in PBS). Cells were then incubated with primary antibodies in blocking solution at 4°C for overnight, followed by incubation with secondary antibodies (2–3 h, at room temperature). To stain the nucleus and F-actin, Hoechst 33258 (Sigma-Aldrich) and Rhodamine-phalloidin (Cytoskeleton Inc., Denver, CO) were used, respectively. Monoclonal antibody against α -tubulin (1:1000; 12G10) was obtained from Developmental Studies Hybridoma Bank of University of Iowa. Monoclonal antibodies against β -tubulin (1:1000; Tub2.1, Cy3-conjugated, #C4585), tyrosinated tubulin (1:2000; TUB-1A2, #T9028) and acetylated tubulin (1:10000; 6-11B-1, #T6793) were obtained from Sigma-Aldrich. Antibodies against detyrosinated tubulin (1:1000; #AB3201) and kinesin heavy chain (1:50; clone H2, #MAB1614) were purchased from Merck Millipore (Darmstadt, Germany). For secondary antibodies, goat anti-mouse- or anti-rabbit-IgG conjugated to Alexa Fluor dyes (1:1000; Thermo Fisher Scientific) was used.

Cell imaging and data quantification

Images of fixed neurons were obtained under an Axiovert 200 M microscope equipped with AxioCam MRm digital camera (Carl-Zeiss, Oberkochen, Germany), and were analyzed using ImageJ software (National Institutes of Health). In some experiments, a confocal laser scanning microscope (LSM 5 PASCAL; Carl-Zeiss) or ApoTome.2 (Carl-Zeiss) was used to obtain sectionized images (see below). In the analysis of arbor terminals, processes that were more than 20 μ m in length were selected to exclude short protrusions.

Time-lapse imaging of the axonal arbor

For time-lapse imaging, neurons were cultured on glass bottom plates (Iwaki, Chiba, Japan) attached by flexiperm (Sarstedt, Nümbrecht, Germany). Minimal Essential Medium (MEM; Thermo Fisher Scientific) that did not contain Texas Red was used instead of BME. Images were acquired at 10–20 min intervals by using an Axiovert 200 M equipped with MRm monochromatic digital camera (Carl Zeiss). During the imaging, neuron culture was kept at 36.7°C in the stage top incubator (ZILCS; Tokaihit, Shizuoka, Japan), which was supplied with 5% CO₂, set on the scanning stage. Stage position and camera were controlled by AxioVision software (Carl Zeiss). Images were collected randomly from neurons whose axonal

morphology was clearly observed, and degenerating neurons were excluded from the analysis. Axonal growth rate was calculated by differentiating the value of the segment length in each frame. A positive and negative change was defined as ‘elongation’ and ‘retraction’, respectively. In the inhibition of actin turnover, Latrunculin A (WAKO, Osaka, Japan) was added to the medium prior to placing the culture in the chamber.

Chromophore-assisted light inactivation

CGNs were introduced with expression vectors for KR or KR–KLC together with an EGFP plasmid at 2 DIV, and subjected to CALI at 4 or 5 DIV. For CALI experiments, cells were placed in the stage-top incubator, and a small circular area defined by the iris (~100 µm diameter) was illuminated with a 100 W mercury arc lamp (HBO 100) through a 20× objective lens (Plan-Apochromat, NA 0.8) and a band pass filter (Ex BP/565/30) (Carl-Zeiss). To analyze the stability of the arbor terminal, more than half the area from the terminal end of the longer terminal segment was illuminated for 30 s, and monitored at 15-min intervals for 8 h. Time-lapse images of all axonal arbors that did not undergo degeneration were quantified. To remove any position shift, a time-series of axonal arbor images was aligned using StackReg plugin (Philippe Thévenaz, Swiss Federal Institute of Technology Lausanne) of ImageJ before measuring an image-to-image difference in the length of terminal segment.

Analysis of microtubule content

To analyze microtubule content, mCherry–tubulin was expressed in neurons. Neurons were then simultaneously fixed and permeabilized as described previously (Witte et al., 2008) in a solution containing 60 mM Pipes pH 6.9, 25 mM Hepes, 5 mM EGTA, 1 mM MgCl₂, 0.25% glutaraldehyde, 3.7% paraformaldehyde, 3.7% sucrose and 0.1% Triton X-100, for 20 min at room temperature in order to remove unpolymerized tubulins. The mCherry–tubulin signals in each terminal segment (in the 20 µm from the branching point) were quantified.

FRAP analysis of tubulins

For FRAP analysis of tubulins, a confocal microscope (LSM 5 PASCAL, Carl Zeiss) equipped with a 488-nm argon laser was used. CGNs transfected with expression plasmids for EGFP–tubulin and with or without K5H–mCherry was placed in the stage-top incubator as described above. A rectangular region in the pair of axonal terminal segments that was ~10 µm distal from the branching point was analyzed. After photobleaching the region of interest with the 63× objective lens, fluorescence recovery was monitored every 40 s. Data were quantified by using ImageJ. The fluorescence recovery rate was calculated from a single exponential function, as described previously (Hush et al., 1994) by following Eqn 1, where *frap*(*t*) is the recovered fluorescence at each time point and *C*_{eq} is the total amount of complex. The dissociation constant, *k*_{off} was calculated from plots by fitting and used to calculate the half-time of recovery (2).

$$frap(t) = 1 - C_{eq}e^{-k_{off}t} \quad (1)$$

$$t_{1/2} = \frac{\ln 2}{k_{off}} \quad (2)$$

EB3 experiments

CGNs (5 DIV) transfected with EB3 plasmids by the calcium phosphate method were analyzed. For the fixation, neurons were immediately placed in cold methanol for 20 min and rehydrated with PBS. For the live-cell imaging, neurons were placed in the stage-top incubator, and fluorescence images of EB3 particles was obtained with the ApoTome.2 microscope and MRm camera at 3-s intervals under the 63× objective lens. Velocity of EB3 spot was quantified by using Multiple Kymograph plugin (J. Rietdorf and A. Seitz, European Molecular Biology Laboratory) of ImageJ.

Statistical analysis

Compiled data in bar graphs are expressed as mean±s.e.m. We used the two-tailed Student's *t*-test for statistical analysis unless otherwise stated. The levels of significance are indicated as follows: **P*<0.05, ***P*<0.01, ****P*<0.001.

Acknowledgements

We are grateful to Dr Kazuyuki Murase (University of Fukui) and Dr Mitsutoshi Setou (Hamamatsu University School of Medicine) for support, and Dr Tokuichi Iguchi (University of Osaka) for the advice with EB3 experiments. We also thank Drs Tso-Pang Yao, Torsten Wittmann, Michael Davidson and Dorus Gadella for providing constructs.

Competing interests

The authors declare no competing or financial interests.

Author contributions

T.S., K.M., N.S. and Y.K. analyzed axonal morphology and microtubules, and T.I. and M.K. analyzed F-actin. H.T. contributed to the data analysis, and M.S. and Y.K. designed the experiments and wrote the paper.

Funding

This work was supported by a Ministry of Education, Culture, Sports, Science, and Technology (MEXT) KAKENHI Grant-in-Aid for Scientific Research on Innovative Areas, Nanomedicine Molecular Science [grant numbers 24107509 and 26107707 to Y.K.].

Supplementary information

Supplementary information available online at <http://jcs.biologists.org/lookup/doi/10.1242/jcs.183806.supplemental>

References

- Ageta-Ishihara, N., Takemoto-Kimura, S., Nonaka, M., Adachi-Morishima, A., Suzuki, K., Kamijo, S., Fujii, H., Mano, T., Blaeser, F., Chatila, T. A. et al. (2009). Control of cortical axon elongation by a GABA-driven Ca²⁺/calmodulin-dependent protein kinase cascade. *J. Neurosci.* **29**, 13720–13729.
- Ahmad, F. J., Pienkowski, T. P. and Baas, P. W. (1993). Regional differences in microtubule dynamics in the axon. *J. Neurosci.* **13**, 856–866.
- Ahmad, F. J., Hughey, J., Wittmann, T., Hyman, A., Greaser, M. and Baas, P. W. (2000). Motor proteins regulate force interactions between microtubules and microfilaments in the axon. *Nat. Cell Biol.* **2**, 276–280.
- Ahuja, R., Pinyol, R., Reichenbach, N., Custer, L., Klingensmith, J., Kessels, M. M. and Qualmann, B. (2007). Cordon-bleu is an actin nucleation factor and controls neuronal morphology. *Cell* **131**, 337–350.
- Barnes, A. P. and Polleux, F. (2009). Establishment of axon-dendrite polarity in developing neurons. *Annu. Rev. Neurosci.* **32**, 347–381.
- Bastmeyer, M. and O'Leary, D. D. (1996). Dynamics of target recognition by interstitial axon branching along developing cortical axons. *J. Neurosci.* **16**, 1450–1459.
- Baumgart, F., Rossi, A. and Verkman, A. S. (2012). Light inactivation of water transport and protein-protein interactions of aquaporin-Killer Red chimeras. *J. Gen. Physiol.* **139**, 83–91.
- Bilimoria, P. M., de la Torre-Ubieta, L., Ikeuchi, Y., Becker, E. B. E., Reiner, O. and Bonni, A. (2010). A JIP3-regulated GSK3β/DCX signaling pathway restricts axon branching. *J. Neurosci.* **30**, 16766–16776.
- Brown, A., Li, Y., Slaughter, T. and Black, M. M. (1993). Composite microtubules of the axon: quantitative analysis of tyrosinated and acetylated tubulin along individual axonal microtubules. *J. Cell Sci.* **104**, 339–352.
- Coy, D. L., Hancock, W. O., Wagenbach, M. and Howard, J. (1999). Kinesin's tail domain is an inhibitory regulator of the motor domain. *Nat. Cell Biol.* **1**, 288–292.
- Destaing, O., Planus, E., Bouvard, D., Oddou, C., Badowski, C., Bossy, V., Raducanu, A., Fourcade, B., Albiges-Rizo, C. and Block, M. R. (2010). β1A integrin is a master regulator of invadosome organization and function. *Mol. Biol. Cell* **21**, 4108–4119.
- Dunn, S., Morrison, E. E., Liverpool, T. B., Molina-París, C., Cross, R. A., Alonso, M. C. and Peckham, M. (2008). Differential trafficking of Kif5c on tyrosinated and detyrosinated microtubules in live cells. *J. Cell Sci.* **121**, 1085–1095.
- Edson, K. J., Lim, S.-S., Borisy, G. G. and Letourneau, P. C. (1993). FRAP analysis of the stability of the microtubule population along the neurites of chick sensory neurons. *Cell Motil. Cytoskeleton* **25**, 59–72.
- Gallo, G. (2006). RhoA-kinase coordinates F-actin organization and myosin II activity during semaphorin-3A-induced axon retraction. *J. Cell Sci.* **119**, 3413–3423.
- Gallo, G. (2011). The cytoskeletal and signaling mechanisms of axon collateral branching. *Dev. Neurobiol.* **71**, 201–220.
- Gallo, G. and Letourneau, P. C. (1999). Different contributions of microtubule dynamics and transport to the growth of axons and collateral sprouts. *J. Neurosci.* **19**, 3860–3873.
- Gallo, G., Yee, H. F., Jr. and Letourneau, P. C. (2002). Actin turnover is required to prevent axon retraction driven by endogenous actomyosin contractility. *J. Cell Biol.* **158**, 1219–1228.
- Giannone, G., Mège, R.-M. and Thoumine, O. (2009). Multi-level molecular clutches in motile cell processes. *Trends Cell Biol.* **19**, 475–486.
- Gibson, D. A. and Ma, L. (2011). Developmental regulation of axon branching in the vertebrate nervous system. *Development* **138**, 183–195.

- Goldstein, L. S. B.** (2001). Kinesin molecular motors: transport pathways, receptors, and human disease. *Proc. Natl. Acad. Sci. USA* **98**, 6999-7003.
- Gomez, T. M. and Spitzer, N. C.** (1999). In vivo regulation of axon extension and pathfinding by growth-cone calcium transients. *Nature* **397**, 350-355.
- Hammond, J. W., Huang, C.-F., Kaech, S., Jacobson, C., Banker, G. and Verhey, K. J.** (2010). Posttranslational modifications of tubulin and the polarized transport of kinesin-1 in neurons. *Mol. Biol. Cell* **21**, 572-583.
- Hirokawa, N. and Takemura, R.** (2005). Molecular motors and mechanisms of directional transport in neurons. *Nat. Rev. Neurosci.* **6**, 201-214.
- Homma, N., Takei, Y., Tanaka, Y., Nakata, T., Terada, S., Kikkawa, M., Noda, Y. and Hirokawa, N.** (2003). Kinesin superfamily protein 2A (KIF2A) functions in suppression of collateral branch extension. *Cell* **114**, 229-239.
- Hua, J. Y., Smear, M. C., Baier, H. and Smith, S. J.** (2005). Regulation of axon growth in vivo by activity-based competition. *Nature* **434**, 1022-1026.
- Hush, J. M., Wadsworth, P., Callahan, D. A. and Hepler, P. K.** (1994). Quantification of microtubule dynamics in living plant cells using fluorescence redistribution after photobleaching. *J. Cell Sci.* **107**, 775-784.
- Hutchins, B. I.** (2010). Competitive outgrowth of neural processes arising from long-distance cAMP signaling. *Sci. Signal.* **3**, jc1.
- Hutchins, B. I. and Kalil, K.** (2008). Differential outgrowth of axons and their branches is regulated by localized calcium transients. *J. Neurosci.* **28**, 143-153.
- Ito-Ishida, A., Miyazaki, T., Miura, E., Matsuda, K., Watanabe, M., Yuzaki, M. and Okabe, S.** (2012). Presynaptically released Cbln1 induces dynamic axonal structural changes by interacting with GluD2 during cerebellar synapse formation. *Neuron* **76**, 549-564.
- Jacobson, C., Schnapp, B. and Banker, G. A.** (2006). A change in the selective translocation of the Kinesin-1 motor domain marks the initial specification of the axon. *Neuron* **49**, 797-804.
- Janke, C. and Bulinski, J. C.** (2011). Post-translational regulation of the microtubule cytoskeleton: mechanisms and functions. *Nat. Rev. Mol. Cell Biol.* **12**, 773-786.
- Kalil, K. and Dent, E. W.** (2014). Branch management: mechanisms of axon branching in the developing vertebrate CNS. *Nat. Rev. Neurosci.* **15**, 7-18.
- Kater, S. B. and Mills, L. R.** (1991). Regulation of growth cone behavior by calcium. *J. Neurosci.* **11**, 891-899.
- Kimura, T., Watanabe, H., Iwamatsu, A. and Kaibuchi, K.** (2005). Tubulin and CRMP-2 complex is transported via Kinesin-1. *J. Neurochem.* **93**, 1371-1382.
- Konishi, Y. and Setou, M.** (2009). Tubulin tyrosination navigates the kinesin-1 motor domain to axons. *Nat. Neurosci.* **12**, 559-567.
- Konishi, Y., Stegmüller, J., Matsuda, T., Bonni, S. and Bonni, A.** (2004). Cdh1-APC controls axonal growth and patterning in the mammalian brain. *Science* **303**, 1026-1030.
- Kubota, K., Seno, T. and Konishi, Y.** (2013). A low-density culture method of cerebellar granule neurons with paracrine support applicable for the study of neuronal morphogenesis. *Brain Res.* **1539**, 15-23.
- Lewis, T. L., Jr., Courchet, J. and Polleux, F.** (2013). Cell biology in neuroscience: cellular and molecular mechanisms underlying axon formation, growth, and branching. *J. Cell Biol.* **202**, 837-848.
- Maday, S., Twelvetrees, A. E., Moughamian, A. J. and Holzbaur, E. L. F.** (2014). Axonal transport: cargo-specific mechanisms of motility and regulation. *Neuron* **84**, 292-309.
- Meyer, M. P. and Smith, S. J.** (2006). Evidence from in vivo imaging that synaptogenesis guides the growth and branching of axonal arbors by two distinct mechanisms. *J. Neurosci.* **26**, 3604-3614.
- Nakata, T. and Hirokawa, N.** (2003). Microtubules provide directional cues for polarized axonal transport through interaction with kinesin motor head. *J. Cell Biol.* **162**, 1045-1055.
- Nakata, T., Niwa, S., Okada, Y., Perez, F. and Hirokawa, N.** (2011). Preferential binding of a kinesin-1 motor to GTP-tubulin-rich microtubules underlies polarized vesicle transport. *J. Cell Biol.* **194**, 245-255.
- Nishiyama, H., Fukaya, M., Watanabe, M. and Linden, D. J.** (2007). Axonal motility and its modulation by activity are branch-type specific in the intact adult cerebellum. *Neuron* **56**, 472-487.
- Okamoto, M., Iguchi, T., Hattori, T., Matsuzaki, S., Koyama, Y., Taniguchi, M., Komada, M., Xie, M.-J., Yagi, H., Shimizu, S. et al.** (2015). DBZ regulates cortical cell positioning and neurite development by sustaining the anterograde transport of Lis1 and DISC1 through control of Ndel1 dual-phosphorylation. *J. Neurosci.* **35**, 2942-2958.
- Peris, L., Wagenbach, M., Lafanechère, L., Brocard, J., Moore, A. T., Kozielski, F., Job, D., Wordeman, L. and Andrieux, A.** (2009). Motor-dependent microtubule disassembly driven by tubulin tyrosination. *J. Cell Biol.* **185**, 1159-1166.
- Portera-Cailliau, C., Weimer, R. M., De Paola, V., Caroni, P. and Svoboda, K.** (2005). Diverse modes of axon elaboration in the developing neocortex. *PLoS Biol.* **3**, e272.
- Reed, N. A., Cai, D., Blasius, T. L., Jih, G. T., Meyhofer, E., Gaertig, J. and Verhey, K. J.** (2006). Microtubule acetylation promotes kinesin-1 binding and transport. *Curr. Biol.* **16**, 2166-2172.
- Riedl, J., Crevenna, A. H., Kessenbrock, K., Yu, J. H., Neukirchen, D., Bista, M., Bradke, F., Jenne, D., Holak, T. A., Werb, Z. et al.** (2008). Lifeact: a versatile marker to visualize F-actin. *Nat. Methods* **5**, 605-607.
- Robson, S. J. and Burgoyne, R. D.** (1989). Differential localisation of tyrosinated, detyrosinated, and acetylated alpha-tubulins in neurites and growth cones of dorsal root ganglion neurons. *Cell Motil. Cytoskeleton* **12**, 273-282.
- Ruthel, G. and Hollenbeck, P. J.** (2000). Growth cones are not required for initial establishment of polarity or differential axon branch growth in cultured hippocampal neurons. *J. Neurosci.* **20**, 2266-2274.
- Salinas, S., Bilsland, L. G. and Schiavo, G.** (2008). Molecular landmarks along the axonal route: axonal transport in health and disease. *Curr. Opin. Cell Biol.* **20**, 445-453.
- Sano, Y., Watanabe, W. and Matsunaga, S.** (2014). Chromophore-assisted laser inactivation - towards a spatiotemporal-functional analysis of proteins, and the ablation of chromatin, organelle and cell function. *J. Cell Sci.* **127**, 1621-1629.
- Seetapun, D. and Odde, D. J.** (2010). Cell-length-dependent microtubule accumulation during polarization. *Curr. Biol.* **20**, 979-988.
- Shelly, M., Lim, B. K., Cancedda, L., Heilshorn, S. C., Gao, H. and Poo, M.-m.** (2010). Local and long-range reciprocal regulation of cAMP and cGMP in axon/dendrite formation. *Science* **327**, 547-552.
- Spillane, M., Ketschek, A., Jones, S. L., Korobova, F., Marsick, B., Lanier, L., Svitkina, T. and Gallo, G.** (2011). The actin nucleating Arp2/3 complex contributes to the formation of axonal filopodia and branches through the regulation of actin patch precursors to filopodia. *Dev. Neurobiol.* **71**, 747-758.
- Spillane, M., Ketschek, A., Donnelly, C. J., Pacheco, A., Twiss, J. L. and Gallo, G.** (2012). Nerve growth factor-induced formation of axonal filopodia and collateral branches involves the intra-axonal synthesis of regulators of the actin-nucleating Arp2/3 complex. *J. Neurosci.* **32**, 17671-17689.
- Stepanova, T., Slemmer, J., Hoogenraad, C. C., Lansbergen, G., Dortland, B., De Zeeuw, C. I., Grosveld, F., van Cappellen, G., Akhmanova, A. and Galjart, N.** (2003). Visualization of microtubule growth in cultured neurons via the use of EB3-GFP (end-binding protein 3-green fluorescent protein). *J. Neurosci.* **23**, 2655-2664.
- Stettler, D. D., Yamahachi, H., Li, W., Denk, W. and Gilbert, C. D.** (2006). Axons and synaptic boutons are highly dynamic in adult visual cortex. *Neuron* **49**, 877-887.
- Strasser, G. A., Rahim, N. A., VanderWaal, K. E., Gertler, F. B. and Lanier, L. M.** (2004). Arp2/3 is a negative regulator of growth cone translocation. *Neuron* **43**, 81-94.
- Tang, F. and Kalil, K.** (2005). Netrin-1 induces axon branching in developing cortical neurons by frequency-dependent calcium signaling pathways. *J. Neurosci.* **25**, 6702-6715.
- Witte, H., Neukirchen, D. and Bradke, F.** (2008). Microtubule stabilization specifies initial neuronal polarization. *J. Cell Biol.* **180**, 619-632.
- Yu, W. and Baas, P. W.** (1994). Changes in microtubule number and length during axon differentiation. *J. Neurosci.* **14**, 2818-2829.
- Yu, W., Qiang, L., Solowska, J. M., Karabay, A., Korulu, S. and Baas, P. W.** (2008). The microtubule-severing proteins spastin and katanin participate differently in the formation of axonal branches. *Mol. Biol. Cell* **19**, 1485-1498.